

Elsevier required licence: © <2022>. This manuscript version is made available under the CC-BY-NC-ND 4.0 license <http://creativecommons.org/licenses/by-nc-nd/4.0/>

The definitive publisher version is available online at

[\[https://www.sciencedirect.com/science/article/abs/pii/S0017931021015465?via%3Dihub\]](https://www.sciencedirect.com/science/article/abs/pii/S0017931021015465?via%3Dihub)

Topological design of hierarchical thermoelastic structures

Yongfeng Zheng^{a,c}, Zhen Luo^{b*}, Yanzheng Wang^c, Jinping Qu^{a*}, Chuanzeng Zhang^c

^a National Engineering Research Center of Novel Equipment for Polymer Processing, Key Laboratory of Polymer Processing Engineering (South China University of Technology), Ministry of Education, Guangdong Provincial Key Laboratory of Technique and Equipment for Macromolecular Advanced Manufacturing, School of Mechanical and Automotive Engineering, South China University of Technology, Guangzhou 510641, China.

^b School of Mechanical and Mechatronic Engineering, University of Technology Sydney, NSW 2007, Australia.

^c Department of Civil Engineering, University of Siegen, D-57068 Siegen, Germany.

* Corresponding author. E-mail address: zhen.luo@uts.edu.au, jpqu@scut.edu.cn.

Abstract: This study proposes a new design method to perform the topological design of hierarchical thermoelastic structures for thermal insulation. Firstly, a design strategy with three layers including macro-, meso- and micro-layers is presented. The macroscopic structures are formed by periodically arranged mesoscopic structures, whose topological configurations are determined by the material microstructures provided at the micro-level. The microstructures and mesoscopic structures are independent of the optimization. Then, the floating projection technique is employed to find the optimal distribution path of insulation materials, without penalization used in the conventional density-based methods. The objective function is defined by maximizing the thermal compliance, subjected to the volume constraint that is added to the objective function through Lagrange multiplier. The sensitivity derivation and the algorithm implementation are given in detail. Finally, some numerical examples are presented to illustrate the advantages of the proposed method, and the design robustness of the topological results in both the damage tolerance and load position offset.

Keywords: Topology optimization, floating projection, material mechanics, thermal insulation, hierarchical structures.

1. Introduction

Most of the existing literature referring to heat problems have widely investigated the topological design for the maximum heat transfer, while thermal insulation has not received as much attention. Actually, heat preservation design is also important in civil and mechanical engineering, especially in the area of building technology (Bruggi and Cinquini, 2011; Xia et al., 2018; Zhuang et al., 2007). Compared to the conventional continuous solids, hierarchical structures possess many favorable features such as lightweight, high energy absorption, high wave absorption, impact resistance, and vibration isolation (Jansen and Pierard, 2020). Hence, hierarchical structures are attracting extensive attentions in engineering. Although there have been many methods investigated various hierarchical structures in the past, they were associated with some drawbacks. The previous studies with scale separations were mostly limited to the design of periodic and lattice structures (Wang et al., 2017; Wu et al., 2019), rather than the rigorous hierarchical structures. The existing works with the homogenization methods were mostly two-scale designs (Vicente et al., 2016; Zheng et al., 2019), which are inefficient for the design of hierarchical structures with three or more scales. Additionally, multiscale hierarchical structures considering thermal insulation are relatively rare. Topology

optimization is an efficient numerical tool and widely utilized to design advanced structures and material microstructures (Bendsøe and Sigmund, 2013; Sigmund, 2020; Xue et al., 2017; Zhang et al., 2019; Zhang et al., 2021; Zheng et al., 2020; Zheng et al., 2021). As a recently developed method, the floating projection topology optimization (FPTO) method (Huang, 2020b) exhibits some advantages such as good stability, smooth boundary and not easy to fall into the local optimum, which shows us a new vision on implementing the topology optimization algorithm.

This study will propose a new design strategy to perform topological design of hierarchical thermoelastic structures for thermal insulation (Zhou et al., 2012). The insulated structure include three scales or levels, namely, the micro-, meso- and macro-structural scales. The macrostructures are to be optimized and formed by the periodic mesoscopic structures, the mesoscopic structures are composed of some non-periodic microstructures, which are provided at the micro-level. Four different types of the microstructures can be selected in this study. The structural configurations at the meso- and micro-levels are independent of the optimization, and the homogenization method bridges the macroscopic equivalent thermoelastic properties of the mesoscopic structures. This design strategy is tested on the implementing of thermal insulation problem, where the FPTO is employed to find the optimal distributions of insulation materials. The objective function is to maximize the thermal compliance, subjected to the volume constraint that is added to the objective function by using Lagrange multiplier. A heuristic optimality criterion is derived to iteratively update the design variables. Some numerical examples are presented to discuss the influences of material properties and topological configurations of the mesoscopic structures, on the hierarchical designs.

2. Mathematical modeling and design strategy

The pros and cons of thermal performance are usually characterized by the thermal compliance, a bigger thermal compliance generates a worse heat conduction efficiency (Gao and Zhang, 2010; Gersborg-Hansen et al., 2006). Therefore, the present topology optimization in thermal insulation is to maximize the thermal compliance under a given material usage. Based on the FPTO method, the mathematical modeling can be stated as (Bruggi and Cinquni, 2011)

$$\begin{aligned}
 & \text{Maximize: } C = \mathbf{T}^T \mathbf{K} \mathbf{T} \\
 & \text{Subject to: } \sum_{e=1}^N (1 - \rho_e) V_e \leq V_f \\
 & \mathbf{K} \mathbf{T} = \mathbf{P} \\
 & 0 < \rho_{\min} \leq \rho_e \leq 1
 \end{aligned} \tag{1}$$

In Eq. (1), C is the thermal compliance, \mathbf{T} is the structural temperature matrix, \mathbf{K} is the global heat conductivity matrix, N is the elemental number discretized in the design domain, ρ_e is the elemental density to be determined during optimization, V_e is the elemental volume, V_f is the upper limit of the prescribed volume fraction. \mathbf{P} is the thermal load vector, ρ_{\min} is a small positive value (0.001 in this paper), to avoid the computational singularities of the heat conductivity matrix, $\rho_e = 0$ denotes the insulation fraction and $\rho_e = 1$ refers to the conductive phase.

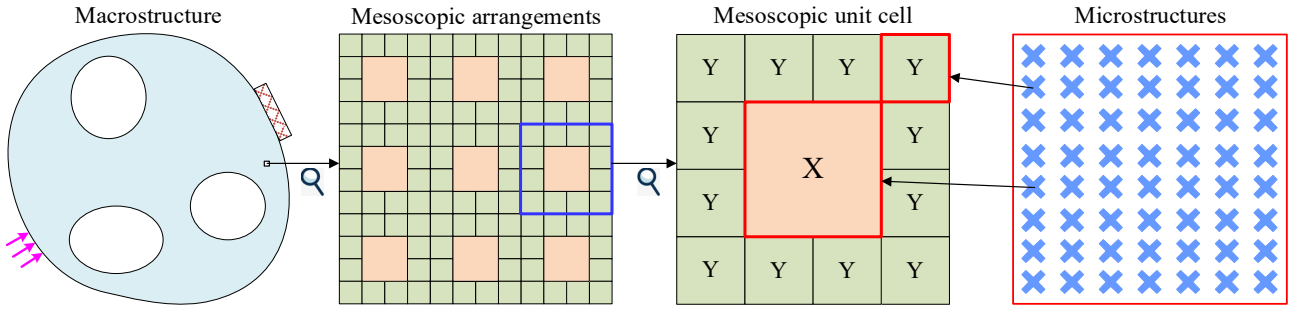


Fig. 1. Illustration for the design strategy with three layers

This study proposes a novel design strategy to obtain hierarchical structures with three layers at the macro-, meso- and micro-levels, as depicted in Fig. 1. The macroscopic structure is to be optimized, which is formed by periodically arranged mesoscopic structures XY, X and Y in the meso-structure usually have different topologies for a multifunctional macrostructure, since different configurations represent different properties. Moreover, X and Y are some classical microstructures selected from the micro-layer. It is noted that the mesoscopic structures and microstructures are independent of the optimization, and their macroscopic properties and topological configurations are known in advance.

Table 1. The considered four microstructures

Type	A	B	C	D
Porosity	0.70	0.70	0.70	0.70
PUC				
$\begin{bmatrix} K_{11}^H & K_{12}^H \\ K_{21}^H & K_{22}^H \end{bmatrix}$	$\begin{bmatrix} 0.4989 & 0.0660 \\ 0.0660 & 0.4989 \end{bmatrix}$	$\begin{bmatrix} 0.4995 & -0.0660 \\ -0.0660 & 0.4995 \end{bmatrix}$	$\begin{bmatrix} 0.4956 & 0 \\ 0 & 0.4956 \end{bmatrix}$	$\begin{bmatrix} 0.5133 & 0 \\ 0 & 0.5133 \end{bmatrix}$

To illustrate the feasibility of the design strategy in obtaining hierarchical structures for thermal insulation, this study mainly considers four microstructures in the microstructural library. Their periodic unit cell (PUC) and effective macroscopic properties are listed in Table 1, the calculations in macroscopic properties are based on the dimensionless thermal conductivity 1. For configurations A~D, their thermal conductivity tensors in the horizontal and vertical directions are the same. However, the coupling (off-diagonal) terms are equal to 0 in the configurations C and D, non-zero and opposite in the configurations A and B. Due to the possibility of different macroscopic properties induced by the same topologies and porosities, this study considers the same geometrical sizes in each microstructure, to make fair comparisons.

Fig. 2 depicts the normalized equivalent thermal conductivities of the microstructures A~D, where 20 samples with 0.5 interval are used to simulate the normalized conductivities. K_{11} and K_{22} denote the thermal conductivities of the porous materials in the x - and y - directions, respectively. K_{12} and K_{21} are the coupling conductivities of the porous materials along with the xy - and yx -directions, respectively. K_s is the thermal conductivity of solid material.

As depicted in Fig. 2, as the material density increases, the conductivities of the four porous microstructures in the x - and y - directions are also increase accordingly, and their changing trends

show the same parabolic shape. Furthermore, the thermal coupling tensors of K_{12} and K_{21} in A configuration increase first and then decrease, but they decrease first and then increase in B configuration, their inflection points are about the density value of 0.75.

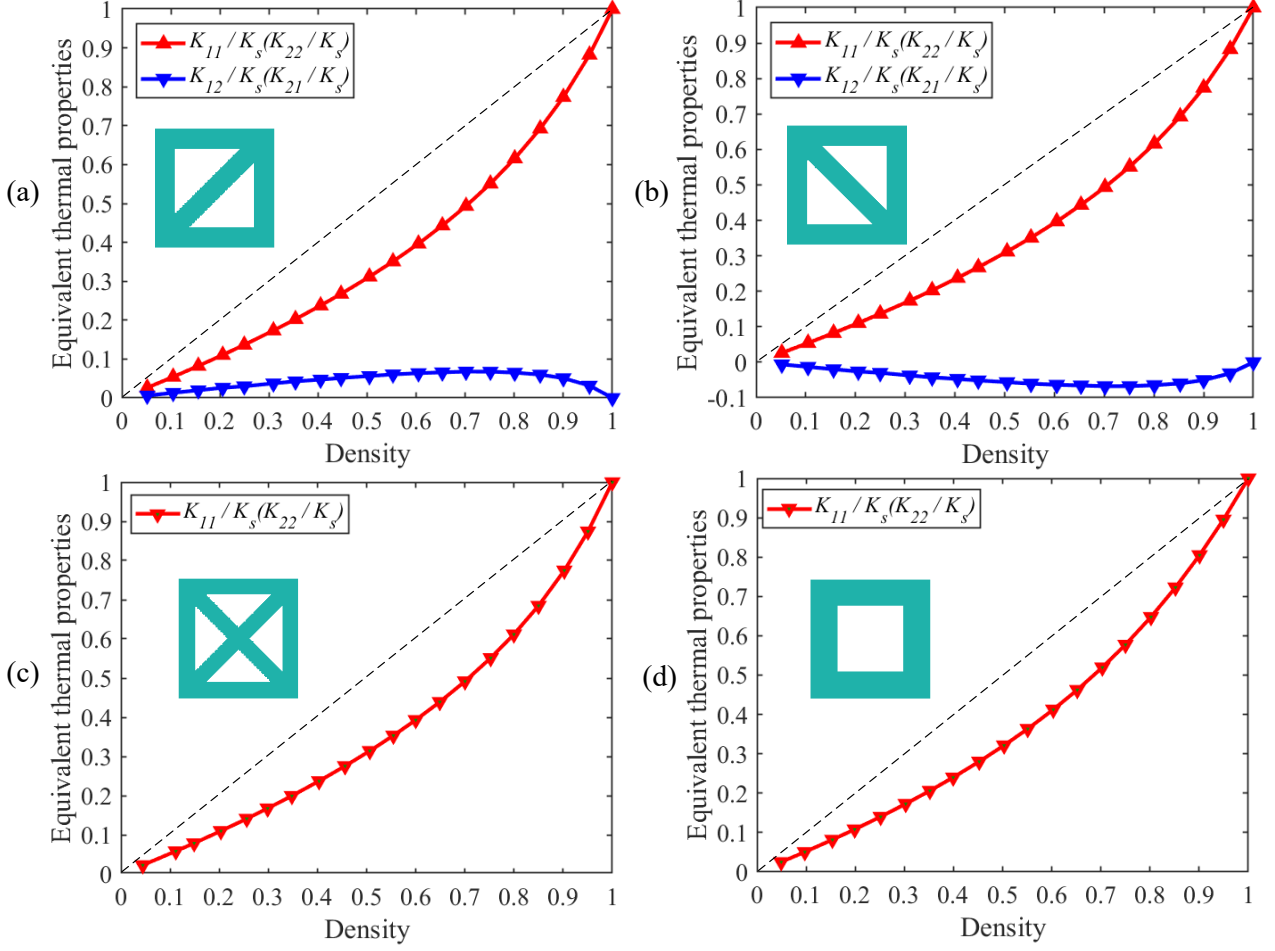


Fig. 2. Normalized equivalent thermal conductivities of the microstructures A-D

3. Sensitivity analysis and algorithm implementation

To utilize the mature optimization algorithm solving the problem defined in Eq. (1), the derivative of the objective function with respect to the design variables should be computed (Takezawa et al., 2014), such as

$$\frac{\partial C}{\partial \rho_e} = \frac{\partial}{\partial \rho_e} (\mathbf{T}^T \mathbf{K} \mathbf{T}) = \mathbf{P}^T \frac{\partial \mathbf{T}}{\partial \rho_e} \quad (2)$$

By differentiating the design variables on both sides of the equality constraint listed in Eq. (1), the following relations can be obtained.

$$\begin{aligned} \frac{\partial \mathbf{P}}{\partial \rho_e} &= \frac{\partial (\mathbf{K} \mathbf{T})}{\partial \rho_e} = \frac{\partial \mathbf{K}}{\partial \rho_e} \mathbf{T} + \frac{\partial \mathbf{T}}{\partial \rho_e} \mathbf{K} \Rightarrow 0 = \frac{\partial \mathbf{K}}{\partial \rho_e} \mathbf{T} + \frac{\partial \mathbf{T}}{\partial \rho_e} \mathbf{K} \\ &\Rightarrow \frac{\partial \mathbf{T}}{\partial \rho_e} = -\mathbf{K}^{-1} \frac{\partial \mathbf{K}}{\partial \rho_e} \mathbf{T} \Rightarrow \mathbf{P}^T \frac{\partial \mathbf{T}}{\partial \rho_e} = -\mathbf{P}^T \mathbf{K}^{-1} \frac{\partial \mathbf{K}}{\partial \rho_e} \mathbf{T} \end{aligned} \quad (3)$$

By combining Eqs. (2) and (3), the sensitivity information can be rewritten as

$$\frac{\partial C}{\partial \rho_e} = -\mathbf{P}^T \mathbf{K}^{-1} \frac{\partial \mathbf{K}}{\partial \rho_e} \mathbf{T} = -\mathbf{T}^T \frac{\partial \mathbf{K}}{\partial \rho_e} \mathbf{T} = -\sum_{e=1}^N \mathbf{t}_e^T \mathbf{K}_e \mathbf{t}_e \quad (4)$$

According to the material interpolation scheme used in the density-based method, the heat conduction

matrix \mathbf{K}_e in each element should be interpolated by

$$\mathbf{K}_e = \rho_e \mathbf{K}_0 \quad (5)$$

where \mathbf{K}_0 represents the equivalent heat conductivity properties of the considered mesoscopic structures. It is noted that this paper employs the floating projection technique to form the structural topologies, so the penalty factor is unnecessary in the calculation of \mathbf{K}_e . By substituting Eq. (5) into Eq. (4), and take into account the maximization of the objective function, the sensitivity information can be finally written as

$$\frac{\partial C}{\partial \rho_e} = \sum_{e=1}^N \mathbf{t}_e^T \mathbf{K}_0 \mathbf{t}_e \quad (6)$$

To stably update the design variables, the elemental sensitivity in current iteration is obtained by averaging with its previous values, such as

$$\left(\frac{\partial C^i}{\partial \rho_e} + \frac{\partial C^{i-1}}{\partial \rho_e} \right) / 2 \rightarrow \frac{\partial C^i}{\partial \rho_e} \quad (7)$$

where the superscript i denotes the current iteration number. According to the Karush-Kuhn-Tucker (KKT) conditions used in mathematical programming (Sigmund, 2001), the following formula can be obtained.

$$f = C + \lambda(V - V_0) + \sum_{j=1}^3 \lambda_j (g_j - g_j^*) \quad (8)$$

where λ and λ_j are non-negative Lagrange multipliers corresponding to the constraints listed in Eq. (1), which includes the volume, balance equation, upper and lower bounds of the design variables. Since the balance equation, upper and lower bounds of the design variables will be satisfied automatically during the optimization, the last term in Eq. (8) can be ignored, such as

$$\frac{\partial f}{\partial \rho_e} = \frac{\partial C}{\partial \rho_e} + \lambda \frac{\partial V}{\partial \rho_e} = 0 \quad (9)$$

Furthermore, the heuristic optimality criterion to update the design variables can be expressed as

$$x_e^i = \begin{cases} x_{\min}, & \text{if } x_e^i \leq x_{\min}, \\ \left(-\frac{\partial C / \partial \rho_e}{\lambda \partial V / \partial \rho_e} \right) x_e^{i-1}, & \text{otherwise,} \\ 1, & \text{if } x_e^i \geq 1. \end{cases} \quad (10)$$

where λ can be determined by the bi-section method or the Newton-Raphson method, and the sensitivity of the volume with respect to the design variables is directly given by

$$\partial V / \partial \rho_e = -V_e \quad (11)$$

To suppress the numerical instability such as typical checkerboard pattern and mesh-dependency in the conventional density-based methods, our previous experiences show that the use of the following filter is a simple but efficient way to overcome this problem, such as

$$x_e^{i1} = \sum_{j=1}^N w(r_{ij}) x_e^i / \sum_{j=1}^N w(r_{ij}) \quad (12)$$

where r_{ij} denotes the distance between the centers of the i -th and j -th elements, and w is a weight coefficient calculated by

$$w(r_{ij}) = \begin{cases} r_{\min} - r_{ij}, & \text{if } r_{ij} \leq r_{\min}, \\ 0, & \text{if } r_{ij} > r_{\min}, \end{cases} \quad (13)$$

where r_{\min} is the prescribed filter radius.

Although the above-described filter scheme is adopted, the optimized topologies are still filled with some intermediate densities. To overcome this difficulty, the floating projection technique is employed to progressively push the design variables toward 1 and 0, which leads to

$$x_e^{i2} = \frac{\tanh(\beta \cdot th) + \tanh[\beta \cdot (x_e^{i1} - th)]}{\tanh(\beta \cdot th) + \tanh[\beta \cdot (1 - th)]} \quad (13)$$

where $\beta > 0$ denotes the steepness coefficient, th is the floating threshold used to ensure the volume invariance before and after floating. Besides, a move limit should be given to avoid the large changes in the design variables, which is taken as 0.02 in this paper. To gradually push the design variables toward 1 or 0, β usually starts from a small positive value (10^{-6} in this paper), and increases with $\Delta\beta$ (1 in this paper) until the following smooth criterion is satisfied:


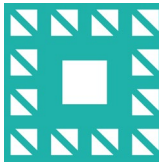
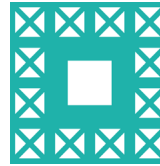

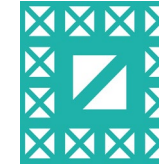

$$\tau = \frac{\sum_{e=1}^N |x_e^i - x_e^{i-1}|}{N} \leq 10^{-3} \quad (14)$$

It should be emphasized that β controls the speed in approaching a 0/1 solution, and it will be stopped to increase once the solution is smooth enough. More information about the smooth representation of structural boundaries in FPTO can be found in reference (Huang, 2020a). Finally, the whole algorithm will be ended until stricter convergence criteria than Eq. (14), $\tau \leq 10^{-4}$ is satisfied.

4. Numerical examples

This section considers three cases to illustrate the insulation performance of the considered six mesoscopic structures, which are listed in Table 2. As listed in Table 2, the thermal conductivities in the horizontal and vertical directions are the same for each mesoscopic structure. If the considered structures are symmetrical, the coupling terms K_{12}^H and K_{21}^H are equal to 0. On the contrary, both of them are positive in A-configurations and negative in AB and B-configurations.

Table 2. The considered six mesoscopic structures

Porosity	0.70	0.70	0.70	0.70	0.70	0.70
Type	DA	DB	DC	AB	AC	AD
PUC						
$\begin{bmatrix} K_{11}^H & K_{12}^H \\ K_{21}^H & K_{22}^H \end{bmatrix}$	$\begin{bmatrix} 0.4989 & 0.0490 \\ 0.0490 & 0.4989 \end{bmatrix}$	$\begin{bmatrix} 0.4995 & -0.0486 \\ -0.0486 & 0.4995 \end{bmatrix}$	$\begin{bmatrix} 0.4958 & 0 \\ 0 & 0.4958 \end{bmatrix}$	$\begin{bmatrix} 0.4920 & -0.0322 \\ -0.0322 & 0.4920 \end{bmatrix}$	$\begin{bmatrix} 0.4896 & 0.0155 \\ 0.0155 & 0.4896 \end{bmatrix}$	$\begin{bmatrix} 0.5044 & 0.0158 \\ 0.0158 & 0.5044 \end{bmatrix}$

The design domains, boundary conditions and the solid designs of three cases are given in Fig. 3. In all the numerical examples, the geometrical sizes of the design domains are $1\text{m} \times 1\text{m}$, which are discretized by 100×100 quadrilateral four-node elements. The specified volume fractions are 0.4, filter radiuses are 2, the blue color represents that the temperature in those positions is 0K, and the red color denotes where the thermal loads are applied. In case 1, a concentrated thermal load 100W/m^3 is

applied at the center of the design domain, and the four sides are adiabatic boundaries. In case 2, five thermal loads 30 W/m^2 are symmetrically distributed in the design domain, four corners are set to be adiabatic. In case 3, the bottom side of square plate is evenly heated as 3 W/m^2 , and the top half is adiabatic boundaries. Fig. 4 gives the topological results for all the hierarchical structures, Table 3 lists all the numerical results.

As shown in Fig. 3 and Fig. 4, the solid and porous designs possess clear topologies and smooth boundaries, which illustrate that the FPTO method has good ability to obtain hierarchical thermoelastic structures. In case 1, all topological results exhibit the same configurations. For the solid design and porous DC result, materials are symmetrically distributed in the four corners of the design domain. Besides, other porous designs distribute more materials on the left or right diagonal corners, due to the asymmetry of their micro-structural configurations. It is interesting to find that if the micro-structural configurations are left tilted, more materials will distribute on the right diagonal corner of the design domain to block the heat transfers, and vice versa.

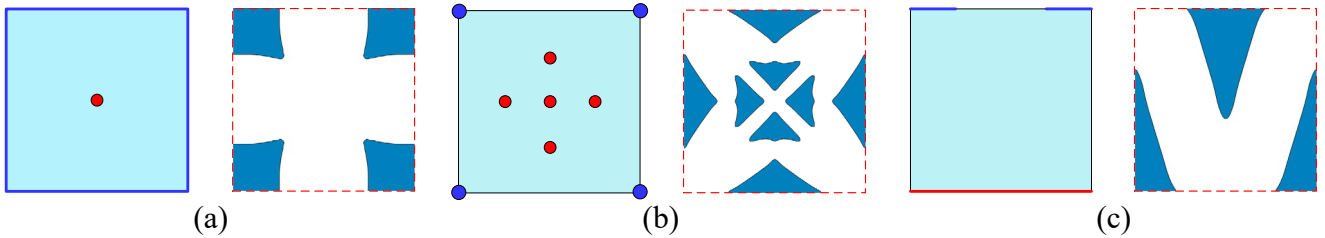


Fig. 3. Design domains and the corresponding solid designs. (a) Case 1; (b) case 2; (c) case 3.

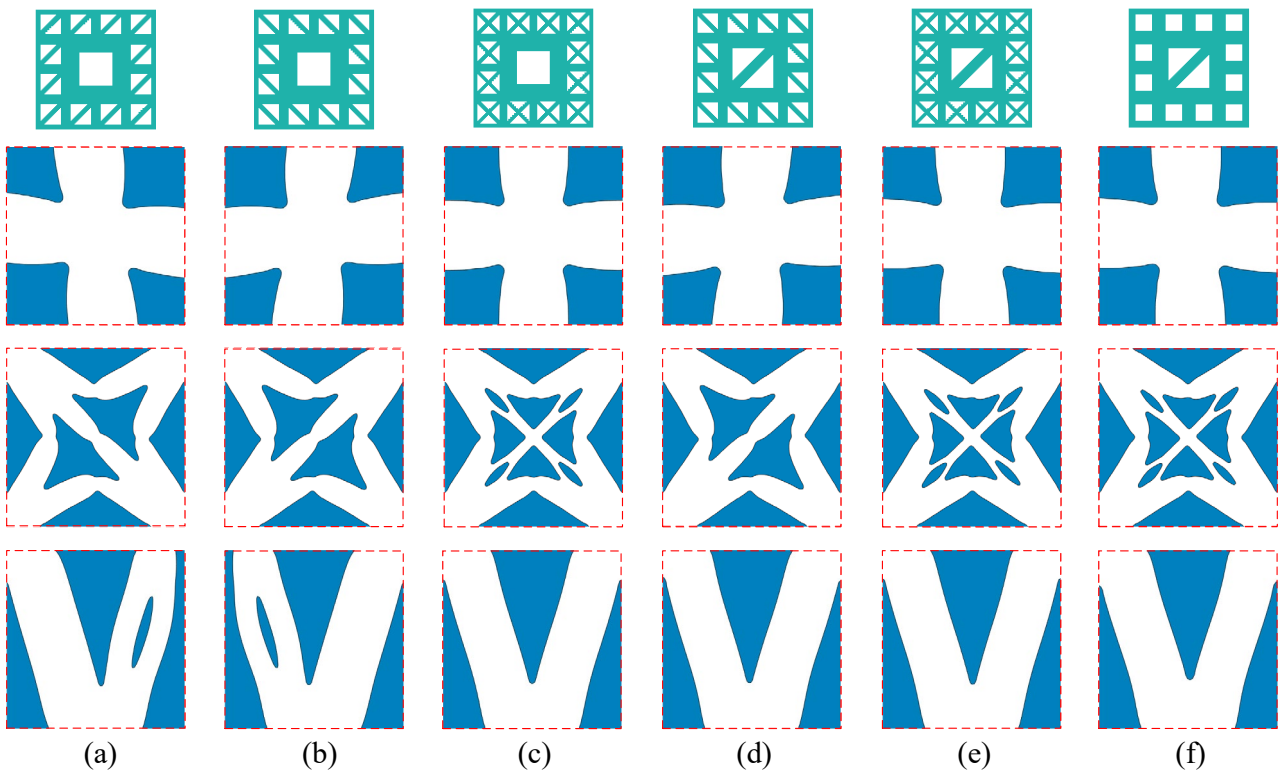


Fig. 4. Topological results for hierarchical structures. (a) DA configuration; (b) DB configuration; (c) DC configuration; (d) AB configuration; (e) AC configuration; (f) AD configuration.

In case 2, solid design is different from all the porous hierarchical designs, some materials are distributed on the four sides, and the remaining materials are symmetrically distributed between

different heat sources to achieve the thermal insulation; for the hierarchical designs, DC, AC and AD results converge to the same topologies, DB and AB configurations are leftly tilted, but DA result is rightly slanted, which demonstrates that the macroscopic topology is more susceptible to the Y configuration in XY.

In case 3, solid design shows an inverted triangle shape on the top, and two right triangles appear on the bottom side, which is true for the hierarchical designs including DC, AB, AC and AD results. For DA and DB results, more materials distribute on the right and left sides of the structure, respectively, due to the larger anisotropy of their microstructures.

As listed in Table 3, values of objective function in all hierarchical designs are bigger than the corresponding solid designs, illustrating that hierarchical designs possess better insulation performance than the corresponding solid designs. The values of AC results in all cases are the largest ones, showing their best performance in thermal insulation, AD results are the worst ones in each case, which indirectly show that the C-type microstructure is more suitable to prevent the heat transfers than others, while the D-type microstructure is the worst one. Furthermore, the sequence of the values in objective function is opposite to the numerical values of the equivalent thermal properties shown in Table 2 (K_{11}^H and K_{22}^H), and the larger thermal constants, the smallest insulation performance. In addition, three cases converge to the final designs with about 100 iterations, illustrating that the FPTO method is efficient to obtain hierarchical thermoelastic structures. The values of the projection coefficient β are equal to 1 and do not need to increase anymore, which shows that the topological boundaries for all cases are always smooth enough during the optimization.

Table 3. Numerical results for all considered cases

Type	Case	Solid	DA	DB	DC	AB	AC	AD
Objective function	1	10055.63	20906.90	20880.57	20984.88	21172.00	21256.27	20634.07
	2	26514.65	55895.19	55823.86	56094.55	56671.17	56800.90	55137.35
	3	35181.38	82987.24	82915.80	83746.82	84532.65	84794.50	82426.09
Iteration number (β)	1	64 (1)	64 (1)	64 (1)	64 (1)	63 (1)	64 (1)	63 (1)
	2	55 (1)	73 (1)	74 (1)	64 (1)	70 (1)	69 (1)	68 (1)
	3	76 (1)	111 (1)	106 (1)	99 (1)	97 (1)	103 (1)	87 (1)

5. Multiple load case and design robustness

This section applies the proposed design strategy to multiple load case and illustrates its design robustness. The geometric size of the design domain is $1\text{m} \times 1\text{m}$, as shown in Fig. 5 (a). Correspondingly, the design domain is discretized by a mesh size of 100×100 quadrilateral grids. There are four points (red color) with heat fluxes $q = 40\text{W/m}^2$ are symmetrically distributed in the design domain, and there is one point (blue color) located at the bottom that has a given temperature $T = 0\text{K}$. It is noting that four heat fluxes are not applied simultaneously, and they belong to two cases P1 and P2, as marked in Fig. 5 (a). For comparisons, Fig. 5 (b~i) gives topological results related to the single load design and all the hierarchical designs (under multi-load condition), in addition to the multi-load design. Table 4 lists the numerical calculation results for all cases.

As shown in Fig. 5, for the single load design, solid materials are separated into five parts and more

materials distribute in the upper part of the design domain, and they are far from the adiabatic point. The remaining designs exhibit the same gate-shaped topologies, although their shapes and sizes are a little different. The topological results illustrate that different micro-structural configurations have little effect on the hierarchical designs under multiple load cases.

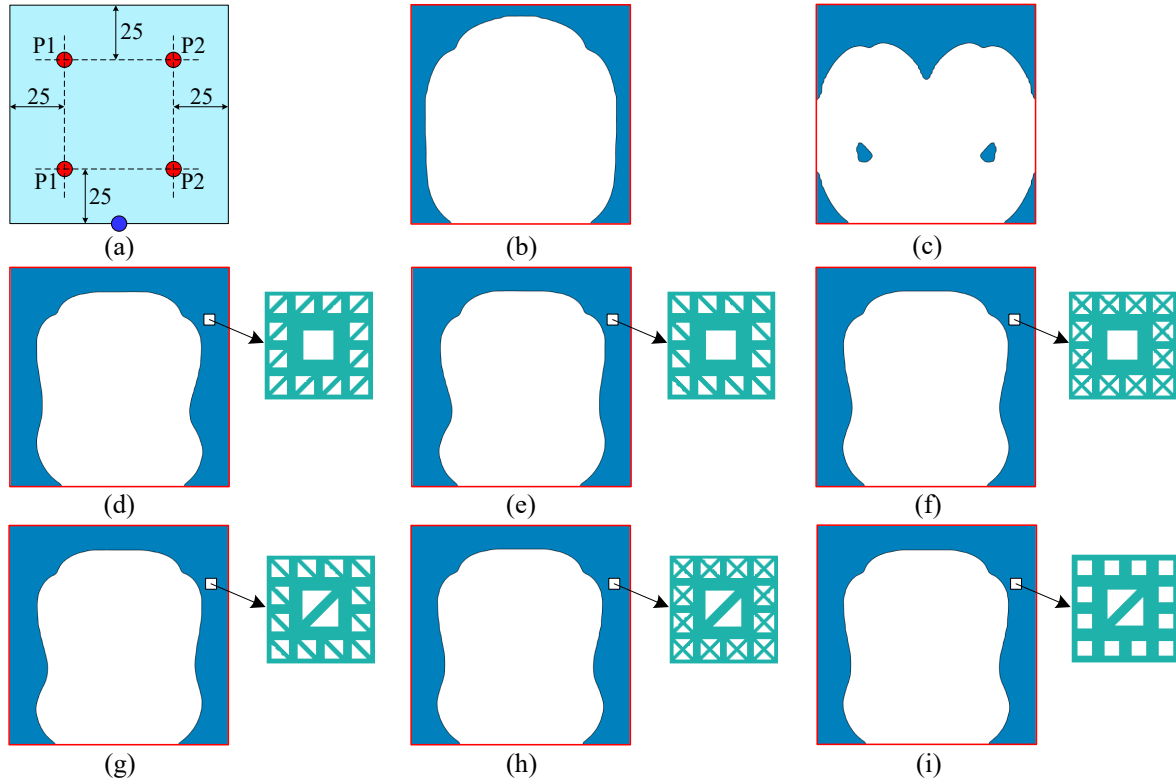


Fig. 5. Design domain and topological results. (a) Design domain under two loads; (b) solid design under multiple loads; (c) solid design under single load; (d) DA configuration; (e) DB configuration; (f) DC configuration; (g) AB configuration; (h) AC configuration; (i) AD configuration.

Table 4. Numerical calculation results for all cases

Type	Normal results	Local failure	Load position offset	Iteration number (β)
Solid design (b)	31354.89	31354.69	30139.55	56 (1)
Solid design (c)	54637.15	54636.74	52285.10	55 (1)
DA	64218.27	64183.85	61358.73	62 (1)
DB	64135.24	64134.15	61279.79	62 (1)
DC	64313.87	64313.54	61462.54	62 (1)
AB	64947.19	64946.09	62062.33	62 (1)
AC	65160.88	65159.21	62268.09	62 (1)
AD	63248.35	63246.98	60440.93	62 (1)

As listed in Table 4, values of the objective function in two solid designs (single load and multiple loads) are smaller than the hierarchical ones, which further explains that hierarchical designs possess better performance in thermal insulation than the corresponding solid designs. The objective function value of single load case is bigger than the multi-load design, since more loads are applied at once. For the hierarchical designs, AC microstructure performs the best performance in thermal insulation because of its biggest value of objective function, while AD configuration is the worst one to achieve thermal insulation among the six hierarchical designs. This phenomenon may be attributed to the

different number of holes inserted into the porous microstructure, we can roughly say that the more holes inserted, the greater the thermal insulation performance, and vice versa.

To further demonstrate the advantages of the proposed design method, we test the robustness of the topological results in both the damage tolerance and load position offset, as illustrated in Fig. 6. Damage tolerance is to ensure that the designed structures are still works as expected (no significant degradation in insulation performance here), even if part of the structure is damaged (Jansen et al., 2014). This is extremely valuable in the aircrafts with high reliability, where local failure usually occurs due to some unexpected events, such as collisions, explosions, fatigue fracture, etc. For simplicity but without loss of generality, a simplified damage model is used, which assumes that a rectangular area located at the upper right corner of the structure is corroded and fractured, and it is randomly given and the materials are removed from this area. For fair comparisons in their insulation performance, all the designed structures shown in Fig. 5 are damaged with the same local failure, we perform finite element analysis to examine how robustness the damaged structures will be. As listed in Table 4, the insulation performance under local failure are smaller than the corresponding normal results, but all the hierarchical design results are larger than the solid design values, which illustrates that the designed hierarchical structures have good abilities to continue working after fracture, showing their better damage robustness than the traditional solid designs.

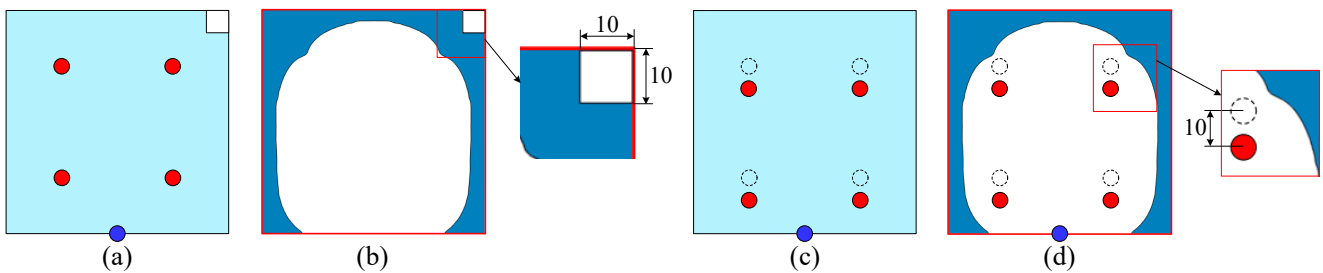


Fig. 6. Illustration for damage tolerance and load position offset. (a) Local failure in design domain; (b) local failure in multi-load design; (c) load position offset in design domain; (d) load position offset in multi-load design.

Another benefit of the designed hierarchical structures is to check their robustness in the load position offset, this situation often occurs in engineering for the following reasons (Li et al., 2020). Firstly, the actual external heat points cannot be guaranteed to be exerted on the specific locations, maybe due to the manufacturing error or installation error. Besides, since the engineering equipment usually work in some complicated conditions, the external heat loads initially applied may shift or offset a little during use, although their magnitude are unchanged. The variations of the heat load positions will make the original topological designs (under specific load positions) inaccurate. Hence, whether the designed structures are insensitive to the variation of the heat load position is also significant in engineering. As listed in Table 4, when position offset exists in all the considered heat points, the thermal insulation performance under all cases are deteriorated, since the numerical results under position offset condition are smaller than the corresponding ones under the specified positions. Besides, all the hierarchical design results are bigger than the solid ones when load position offset exists, which demonstrates that the proposed method is more efficient and robust for insulated structures than the traditional solid designs.

6. Concluding remarks

This study proposes a new method to perform the topological design of hierarchical structures for thermal insulation, it has many advantages such as high efficiency, good connections between different microstructures, macrostructures easily to be manufactured by 3D printing, excellent robustness when suffered from the local damage and load position offset. The FPTO method is demonstrated to be powerful to realize the hierarchical topology optimization. Although the types of the microstructures and mesostructures considered in this study are rather limited, new types of microstructures and mesostructures can be exploited according to the design needs. Then, more suitable mesoscopic structures can be selected to match the specific requirements to the macrostructures. Although the proposed method is tested on the implementing of 2D numerical examples, it can be further applied to other 3D insulation problems, such as the mitigation of the effects of thermal bridges and the heat preservation of the components of modular curtain walls.

Acknowledgements

This research is supported by the Yuesui Joint Foundation for Young Scholars ([Grant no. 2019A1515110183](#)), the Postdoctoral Research Foundation of China ([Grant no. 2020M682699](#)), and the Opening Project of Guangdong Provincial Key Laboratory of Technique and Equipment for Macromolecular Advanced Manufacturing, South China University of Technology, China ([Grant no. 2021kfkt04](#)). Furthermore, the first author would like to thank the China Scholarship Council and the Germany Academic Exchange Service (CSC-DAAD) to jointly support his Postdoctoral Fellowship at the Chair of Structural Mechanics, University of Siegen, Germany.

References

- [Bendsøe, M.P., Sigmund, O., 2013. Topology optimization: theory, methods, and applications. Springer Science & Business Media.](#)
- [Bruggi, M., Cini, C., 2011. Topology Optimization for Thermal Insulation: an Application to Building Engineering. Engineering Optimization 43, 1223-1242.](#)
- [Gao, T., Zhang, W., 2010. Topology optimization involving thermo-elastic stress loads. Structural & Multidisciplinary Optimization 42, 725-738.](#)
- [Gersborg-Hansen, A., Bendsøe, M.P., Sigmund, O., 2006. Topology optimization of heat conduction problems using the finite volume method. Structural & Multidisciplinary Optimization 31, 251-259.](#)
- [Huang, X., 2020a. On smooth or 0/1 designs of the fixed-mesh element-based topology optimization. Advances in Engineering Software 151, 102942.](#)
- [Huang, X., 2020b. Smooth topological design of structures using the floating projection. Engineering Structures 208, 110330.](#)
- [Jansen, M., Lombaert, G., Schevenels, M., Sigmund, O., 2014. Topology optimization of fail-safe structures using a simplified local damage model. Structural & Multidisciplinary Optimization 49, 657-666.](#)
- [Jansen, M., Pierard, O., 2020. A hybrid density/level set formulation for topology optimization of functionally graded lattice structures. Computers & Structures 231, 106205.](#)
- [Li, H., Gao, L., Li, H., Tong, H., 2020. Spatial-varying multi-phase infill design using density-based topology optimization. Computer Methods in Applied Mechanics and Engineering 372, 113354.](#)

- Sigmund, O., 2001. A 99 line topology optimization code written in Matlab. *Structural and Multidisciplinary Optimization* 21, 120-127.
- Sigmund, O., 2020. EML webinar overview: Topology Optimization - Status and Perspectives. *Extreme Mechanics Letters* 39, 100855.
- Takezawa, A., Yoon, G.H., Jeong, S.H., Kobashi, M., Kitamura, M., 2014. Structural topology optimization with strength and heat conduction constraints. *Computer Methods in Applied Mechanics and Engineering* 276, 341-361.
- Vicente, W.M., Zuo, Z.H., Pavanello, R., Calixto, T.K.L., Picelli, R., Xie, Y.M., 2016. Concurrent topology optimization for minimizing frequency responses of two-level hierarchical structures. *Computer Methods in Applied Mechanics & Engineering* 301, 116-136.
- Wang, Y., Xu, H., Pasini, D., 2017. Multiscale isogeometric topology optimization for lattice materials. *Computer Methods in Applied Mechanics & Engineering* 316, 568-585.
- Wu, Z., Xia, L., Wang, S., Shi, T., 2019. Topology optimization of hierarchical lattice structures with substructuring. *Computer Methods in Applied Mechanics and Engineering* 345, 602-617.
- Xia, Q., Shi, T., Xia, L., 2018. Topology optimization for heat conduction by combining level set method and BESO method. *International Journal of Heat and Mass Transfer* 127, 200-209.
- Xue, R., Li, R., Du, Z., Zhang, W., Zhu, Y., Sun, Z., Guo, X., 2017. Kirigami pattern design of mechanically driven formation of complex 3D structures through topology optimization. *Extreme Mechanics Letters* 15, 139-144.
- Zhang, W., Li, D., Kang, P., Guo, X., Youn, S.K., 2019. Explicit topology optimization using IGA-based moving morphable void (MMV) approach. *Computer Methods in Applied Mechanics and Engineering* 360, 112685.
- Zhang, X., Xing, J., Liu, P., Luo, Y., Kang, Z., 2021. Realization of full and directional band gap design by non-gradient topology optimization in acoustic metamaterials. *Extreme Mechanics Letters* 42, 101126.
- Zheng, J., Luo, Z., Jiang, C., Gao, J., 2019. Robust topology optimization for concurrent design of dynamic structures under hybrid uncertainties. *Mechanical Systems and Signal Processing* 120, 540-559.
- Zheng, Y., Wang, Y., Lu, X., Liao, Z., Qu, J., 2020. Evolutionary topology optimization for mechanical metamaterials with auxetic property. *International Journal of Mechanical Sciences* 179, 105638.
- Zheng, Y., Wang, Y., Lu, X., Zheng, J., Qu, J., 2021. Topology optimisation for isotropic mechanical metamaterials considering material uncertainties. *Mechanics of Materials*, 103742.
- Zhou, S., Cadman, J., Chen, Y., Wei, L., Yi, M.X., Huang, X., Appleyard, R., Sun, G., Li, Q., 2012. Design and fabrication of biphasic cellular materials with transport properties - A modified bidirectional evolutionary structural optimization procedure and MATLAB program. *International Journal of Heat & Mass Transfer* 55, 8149-8162.
- Zhuang, C.G., Xiong, Z.H., Ding, H., 2007. A level set method for topology optimization of heat conduction problem under multiple load cases. *Computer Methods in Applied Mechanics & Engineering* 196, 1074-1084.